JOURNAL OF APPLIED ELECTROCHEMISTRY 11 (1981) 551–562

The voltammetric detection of intermediate electrochemical processes related to iron in alkaline aqueous solutions

R. S. SCHREBLER GUZMAN, J. R. VILCHE, A. J. ARVIA

Instituto de Investigaciones Fisicoquímicas Teóricas y Aplicadas (INIFTA), División Electroquímica, Secural 4, Casilla de Correo 16, 1900 La Plata, Argentina

Received 20 October 1980

The application of the triangularly modulated triangular potential sweep technique (TMTPS) to the Fe/alkaline solution interface yields information about the various reactions involving Fe(II) and Fe(III) film-forming species. Qualitative conclusions are derived about the chemical reactions of both $Fe(OH)_2$ and FeOOH with regard to the corresponding ageing processes of these species. The ageing processes appear to be coupled to the overall electrochemical reaction through a composite reaction pattern which, in its simplest form, approaches the square reaction pathway postulated earlier to explain the electrochemical behaviour of the Ni/alkaline solution interface.

1. Introduction

The characteristics of the electrochemical reactions of iron in alkaline solutions, as well as the nature of the products formed, have been studied using many experimental approaches by a large number of authors. The literature has been reviewed recently [1–4].

At Fe/1 N NaOH or Fe/1 N KOH interfaces in which the impurity level is very low (10^{-6} ppm) no corrosion of Fe is observed [5, 6]. The potentiodynamic characteristics of these systems show two anodic and two cathodic current maxima after potential cycling [7]. In the absence of dissolved oxygen the electrochemical behaviour has been explained by invoking a series of successive, conjugated redox couples principally involving Fe(OH), $Fe(OH)_2$ and FeOOH as limiting stoichiometric species [8–12]. Some of these species contribute to the development of a new phase at the electrochemical interface [12–16]. At a pH above 14 the yield of soluble species, such as FeO_2^- or $HFeO_2^-$, also contributes to the overall anodic reaction [1, 8, 10, 17–19] as do processes related to: the oxidation of absorbed and adsorbed hydrogen; the reduction of either an oxygen-containing species or a poison on the electrode; and hydrogen adatom electroformation [7].

At room temperature none of the growth theories currently proposed is capable of describing qualitatively the electroformation of the oxide–hydroxide films on carbon steel [20]: the formation of metastable porous oxides has been assumed [21], as well as an ageing process related to the $Fe/Fe(OH)_2$ interface [8] and composition changes of the mixed oxide layer derived from the current transient behaviour of the Fe/alkaline solution interface [15, 22]. On the other hand, through the use of complex potential perturbation techniques, the occurrence of ageing processes related to the species participating in the various anodic and cathodic reactions was demonstrated [4, 23]. The ageing effects were interpreted as due to the fact that reactants and products involve non-equilibrium structural configurations in both the anodic and cathodic reactions.

The present work attempts to establish some of the intermediate electrochemical processes which are related to the corrosion and passivation of iron in alkaline solutions of different pH and ionic strengths. For this purpose, the electrochemical interface was perturbed with triangularly modulated triangular potential sweeps (TMTPS) [24–26] where the frequency of the modulating signal was several orders of magnitude larger than the base signal frequency, the amplitude of the former being much smaller than that of the latter so as to minimize possible relaxation effects due to the

0021–891X/81/050551–11$03.10/0

anion at the metal surface. When the electrochemical interface is perturbed with TMTPS, the modulating sweep yields directly information on the characteristics of the electrochemical interface, e.g., the stability and kinetic response of the electrochemical species formed, the contribution of anion specific adsorption, the diffuse double-layer relaxation and the double-layer capacitance at the switching potentials.

2. Experimental

The Fe/alkaline solution interface consisted of an iron wire (Johnson Matthey, specpure quality) of 0.05 cm diameter and 0.25 cm^2 apparent area in alkaline solutions prepared from analytical reagent-grade chemicals (Merck) and triply distilled water. The iron electrodes were mechanically polished with emery paper of different grades and with a fine-grade alumina–acetone suspension. Before each potentiodynamic measurement, the electrode was held for 5 min in the hydrogen evolution potential region. The electrochemical cell was completed with a large-area platinum counter electrode and an SCE reference electrode. The electrodes were placed in individual compartments which were connected through fritted glass discs and cup-type glass stopcocks lubricated with the same electrolytic solution. The cell was provided with a protected gas inlet and outlet for the purified nitrogen gas, which flowed through a duct made of Teflon and glass. The solution was saturated with nitrogen before each run and kept continuously under N_2 gas at 25° C. The following electrolyte solutions were used: 1.0 N KOH, 0.1 N KOH, 0.1 N KOH + 0.6 N K_2SO_4 and 0.01 N KOH + 0.66 N K_2SO_4. The electrode potentials are given with reference to the NHE electrode.

The electrochemical interface was first perturbed with a repetitive triangular potential sweep (RTPS) at a preset potential sweep rate ($0.1\ V\ s^{-1} \leqslant v \leqslant 5.0\ V\ s^{-1}$) within fixed cathodic ($E_{s,c}$) and anodic ($E_{s,a}$) switching potentials, their values depending on the electrolyte composition during the time required to attain a stable *E–I* profile. Usually, when a new phase develops under severe anodic polarization, the corresponding reactions are accompanied by a change in the electrode roughness which is reflected in the area of the voltammograms, although when the stabilized *E–I* profile is attained the anodic to cathodic charge ratio is practically equal to one. At this point, it is assumed that the electrode surface has reached a constant real area. Once this was achieved, the triangularly modulated triangular potential sweep (TMTPS) was applied at different base signal sweep rates ($0.1\ V\ s^{-1} \leqslant v_b \leqslant 2.0\ V\ s^{-1}$), modulating signal sweep rates ($0.8\ V\ s^{-1} \leqslant v_m \leqslant 80\ V\ s^{-1}$) and modulating signal amplitudes ($0.03\ V \leqslant \Delta E_m \leqslant 0.36\ V$).

The electro-oxidation or the electro-reduction of adsorbed impurities will result in an excess of either the anodic or cathodic charge respectively, but the contribution of these processes is expected to become insignificant within a few cycles unless large concentrations of dissolved impurities are present in solution. Furthermore, these interferences are less important in alkaline than in acid electrolytes.

3. Results

3.1. *The identification of current peaks and shoulders in the potentiodynamic E–I displays*

Fig. 1 shows three typical *E–I* displays produced either with an RTPS (Fig. 1a) or with the complex sequence of triangular potential perturbations (Figs. 1b and c). The current peaks and shoulders are identified by roman numbers following the nomenclature of previous works [4, 23]. These *E–I* profiles are used to interpret the results obtained with the TMTPS technique. During the positive-going potential excursion the complex contour involves four anodic current peaks (I, II, III and III′), while during the negative-going potential excursion three cathodic current peaks (IV′, IV and V) are observed (Fig. 1a). The numbers with primes refer to shoulders on the right-hand side of definite current peaks and the double-prime numbers to peaks or shoulders produced on the left-hand side of definite current peaks (Figs. 1a–c) either in the RTPS or the STPS after potentiodynamic ageing. The same nomenclature applies to the TMTPS *E–I* profiles. In the following text the roman numbers refer exclusively to the RTPS *E–I* profiles and the roman numbers with either the letter a or c describe the corresponding *E–I* profiles with anodic or cathodic contours in the TMTPS.

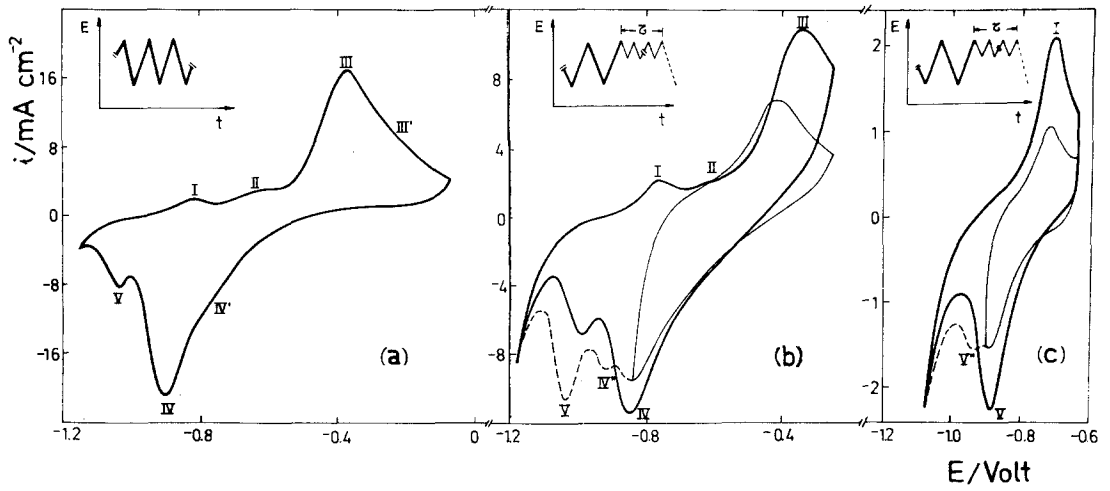

Fig. 1. Potentiodynamic *E–I* contours obtained under different potential perturbation programmes. (a) Stabilized *E–I* profile run with RTPS at 0.2 V s^{-1} in 1 N KOH. (b) Potentiodynamic *E–I* displays run at 0.2 V s^{-1} in 0.1 N KOH with the potential programme depicted in the figure. The broken *E–I* trace was recorded after an intermediate potentiodynamic ageing of 0.5 min between −0.84 V and −0.26 V. (c) Potentiodynamic *E–I* displays obtained in 0.01 N KOH + 0.66 N K_2SO_4 with an intermediate potentiodynamic ageing of 5 min between −1.08 V and −0.64 V.

3.2. *The Fe/1 N KOH interface*

The stabilized RTPS *E–I* profiles (Fig. 2a), recorded using freshly prepared electrodes pretreated with an RTPS for 60 min at 0.2 V s^{-1} between $E_{s,c} = -1.16$ V and $E_{s,a} = -0.06$ V, show a small anodic current peak at ~−0.73 V (peak I), a shoulder at ~−0.6 V (peak II), a large peak at ~−0.33 V (peak III) and two net cathodic current peaks at ~−0.84 V (peak IV) and ~−0.95 V (peak V). A shoulder at ~−0.72 V (peak IV′) is also recorded. At potentials more negative than −1.08 V the evolution of hydrogen from the discharge of water takes place and at potentials more positive than −0.1 V the electrode tends to become passive [4].

The corresponding TMTPS *E–I* display (Fig. 2b) is very sensitive to the characteristics of the potential perturbation. Under properly adjusted perturbation conditions its fine structure can be observed. The definition of the current peak multiplicity is given both by the overall contours of the *E–I* displays and by the *E–I* trace corresponding to each modulating cycle. In any case the optimal conditions for peak multiplicity definition within a particular potential range depend upon the values of v_b, v_m and ΔE_m. The modulating signal reveals various conjugated redox systems along the potential excursion, as well as dramatic differences between the positive- and the negative-going potential excursions. Thus the former exhibits four anodic current peaks: a new one at ~−1.04 V (peak VIa), another at ~−0.72 V (peak Ia), a small one at ~−0.56 V (peak IIa) and a large one at ~−0.31 V (peak IIIa). A small hump (I″a) is also noticed on the left-hand side of current peak Ia. Of all these anodic current peaks, only peaks I″a, Ia and IIa exhibit their corresponding conjugated cathodic current peaks. I″c is hardly distinguishable as a hump at ~−0.96 V. Furthermore, at the positive potential side of peak IIc, it is most probable that two additional cathodic current contributions are included in the −0.85 V to −0.35 V range. The negative-going potential excursion presents a broad anodic current peak (IV′c) whose potential is close to that of current peak II, and two anodic current peaks, one (Va) which is located within the potential range of the anodic hump (VI″a) and another (VIa) at ~−0.93 V. Correspondingly, there is one well-distinguished cathodic current peak (IVc) which coincides with peak IV, and two humps, one (IV′c) located at the right-hand side of peak IVc and another, more clearly distinguishable, (Vc) located at the left-hand side of current peak IVc.

When the RTPS *E–I* profiles at 2 V s^{-1} are restricted between $E_{s,c} = -1.23$ V and $E_{s,a} =$

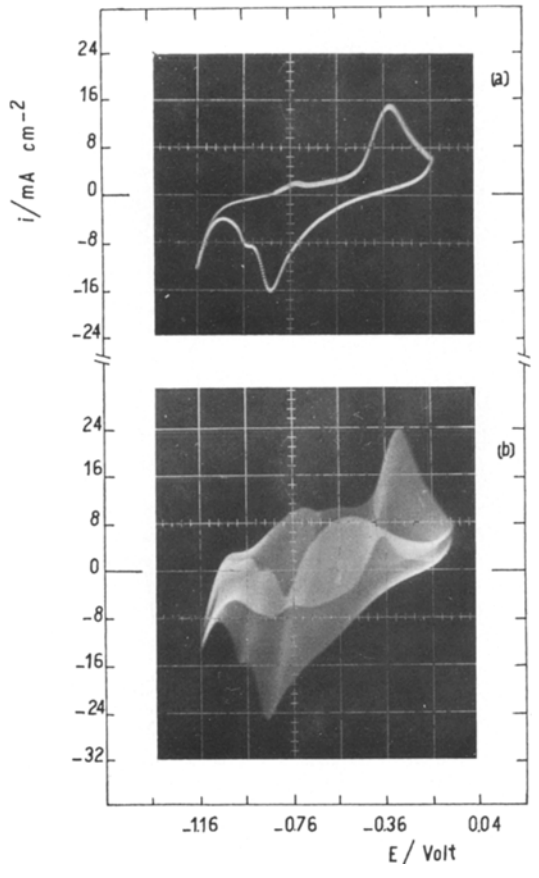

Fig. 2. Comparison between RTPS and TMTPS voltammograms in 1 N KOH solution. (a) $v = 0.2\,V\,s^{-1}$; (b) $v_b = 0.2\,V\,s^{-1}$, $v_m = 20\,V\,s^{-1}$, $\Delta E_m = 0.1\,V$.

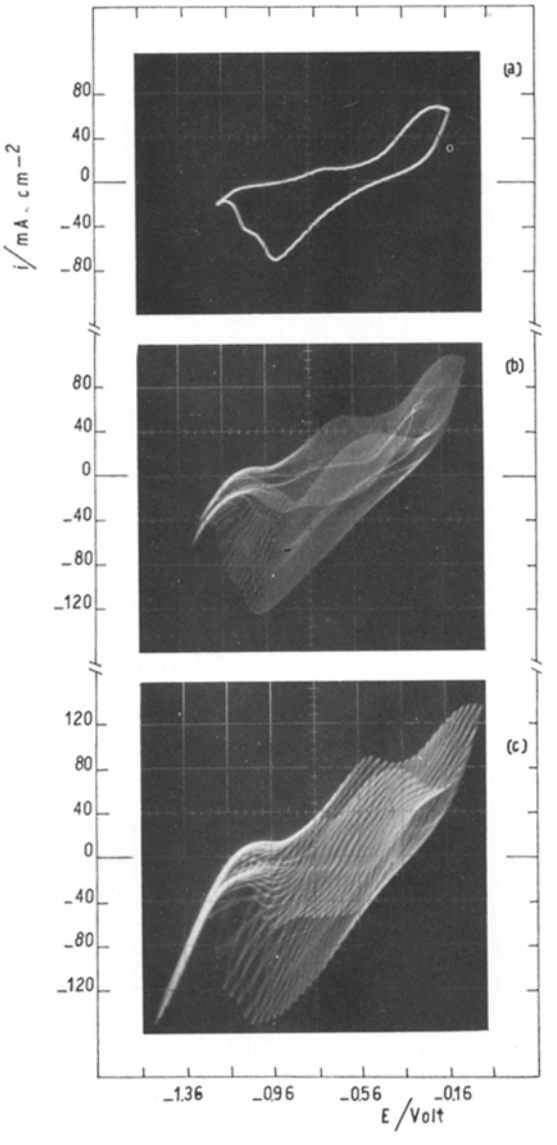

Fig. 3. Comparison between RTPS and TMTPS voltammograms in 1 N KOH. (a) $v = 2\,V\,s^{-1}$; (b) $v_b = 2\,V\,s^{-1}$, $v_m = 50\,V\,s^{-1}$, $\Delta E_m = 0.21\,V$; (c) $v_b = 2\,V\,s^{-1}$, $v_m = 50\,V\,s^{-1}$, $\Delta E_m = 0.36\,V$.

-0.12 V (Fig. 3a) the anodic current peaks shift towards more positive potentials and, simultaneously, the cathodic current peaks shift towards more negative potentials. The complex nature of the current peaks as demonstrated by the corresponding TMTPS runs (Figs. 3b and c) makes it difficult to draw reliable quantitative kinetic relationships from the RTPS data, although from these results one may conclude that these processes at least in part behave as slow electrochemical reactions. When the TMTPS perturbation implies a low v_m/v_b ratio, at a constant ΔE_m (Fig. 4), both the positive- and the negative-going potential excursions show a remarkable change in the electrochemical response of the system to the modulating signal. Thus, in the positive-going potential excursion the reaction response shows an increasing slowness as the potential increases beyond -0.5 V. In the negative-going potential excursion the same effect is observed when the potential decreases below -0.9 V or thereabouts.

To study the E–I characteristics in the potential range of the hydrogen evolution reaction, experiments were made at constant v_b and varying values of ΔE_m and v_m and increasing values of

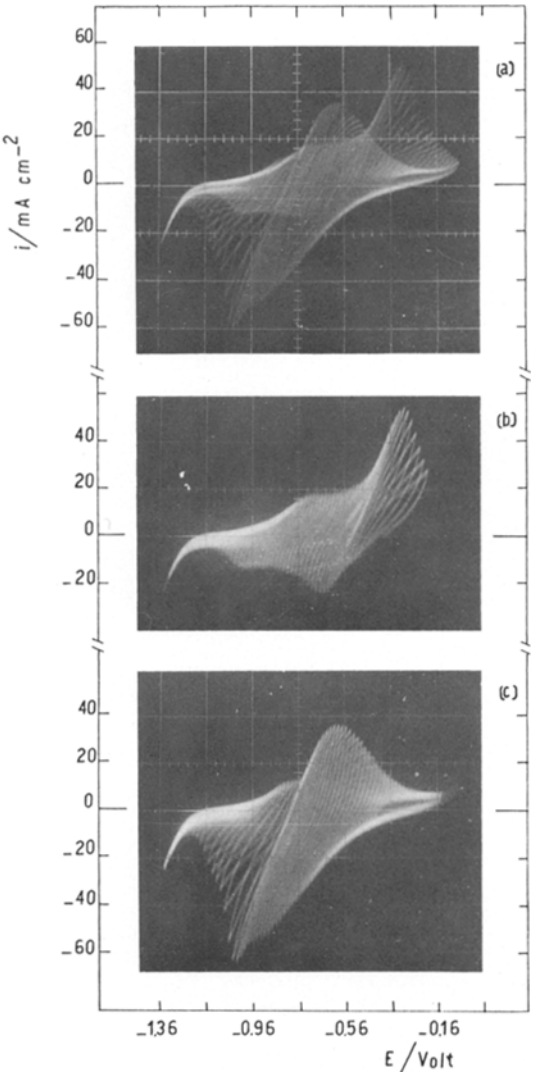

Fig. 4. E–I profiles run with TMTPS in 1 N KOH. v_b = 0.2 V s^{-1}, v_m = 0.8 V s^{-1} and ΔE_m = 0.36 V. (a) Complete E–I contour; (b) positive-going potential excursion; (c) negative-going potential excursion.

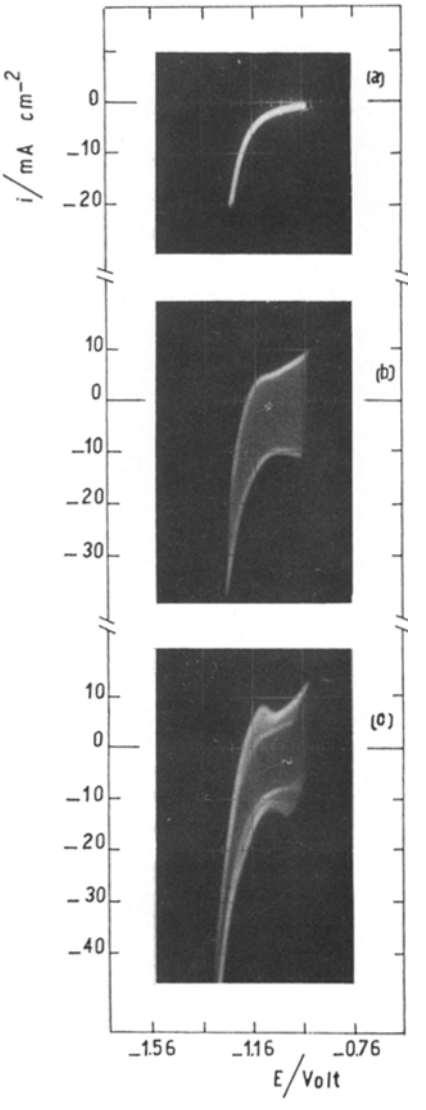

Fig. 5. Comparison between RTPS and TMTPS E–I displays run in the hydrogen evolution potential range. (a) v = 0.2 V s^{-1}; (b) v_b = 0.2 V s^{-1}, v_m = 3 V s^{-1}, ΔE_m = 0.03 V; (c) v_b = 0.2 V s^{-1}, v_m = 3 V s^{-1}; ΔE_m = 0.09 V. 1 N KOH.

$E_{s,c}$ (Fig. 5). The negative-going potential excursion exhibits the cathodic current peak I″c which correlates to current peak I in the RTPS E–I display, but the positive-going potential excursion when $E_{s,c}$ reaches about −1.3 V exhibits a net anodic current peak at ∼−1.12 V. This anodic current peak is probably related to the hardly distinguishable hump at ∼−1.2 V. Both current contributions should be related either to the H_2 evolution or to hydrogen atom intermediates produced during the cathodic reaction. A Faradaic contribution related to the electroreduction of any possible residual oxidized Fe species can, in principle, be disregarded.

The TMTPS E–I displays recorded in a potential region broad enough to include all the processes involved in the active to passive transition of iron, show that the charge passed during the positive-going potential excursion is predominantly anodic, while that recorded during

the returning modulated scan is predominantly cathodic.

3.3. *The Fe/0.1 N KOH interface: the influence of K_2SO_4 addition*

The *E–I* displays recorded under RTPS or TMTPS perturbations with the Fe/0.1 N KOH interface exhibit, in principle, similar features to those described for the Fe/1 N KOH interface, except that the potentials of the different current peaks for the diluted electrolyte are more positive than those corresponding to the 1 N KOH solution (Fig. 6a). By using properly chosen characteristics of the TMTPS perturbation, one particular aspect of the reaction can be emphasized with respect to the other. Thus, for $\Delta E_m = 0.1\,V$, $v_m = 20\,V\,s^{-1}$ and $v_b = 0.2\,V\,s^{-1}$ between $E_{s,c} = -1.2\,V$ and $E_{s,a} = -0.2\,V$, the duration of each modulating cycle is 5×10^{-3} s and during this time a potential range of 1 mV is covered. If one assumes that the average diffusion coefficient of the ionic species in solution is 10^{-5} cm^2 s^{-1}, then, during 5×10^{-3} s, the ions at the interface may move either in or out to a distance of the order of 2.24×10^{-4} cm. This contribution, which corresponds to the relaxation of the diffuse double layer, adds to the abrupt jump in current associated with the charge and discharge of the electrical double layer. This is clearly demonstrated by the current jumps at $E_{s,a}$ and $E_{s,c}$ when the direction of the potential sweep is reversed. Under these circumstances, in the absence of any ohmic polarization the Faradaic contributions remain practically unaltered by the modulating signal. Thus, if only the relaxation of the diffuse double layer contributes during the TMTPS, the *E–I* contours during both the positive- and negative-going potential excursions would be parallel, but when Faradaic reactions are involved, the contours become appreciably distorted. For an infinitely fast, nondiffusion-controlled, film-forming Faradaic process, the charge transfer at any v_m should yield *E–I* contours systematically distributed along the potential axis, but the symmetry is gradually destroyed when the rate of the Faradaic process decreases. The shape of the *E–I* contours should depend, therefore, on the ratio between the rate of the Faradaic process and the frequency and amplitude of the modulating signal.

The TMTPS *E–I* display recorded with a small

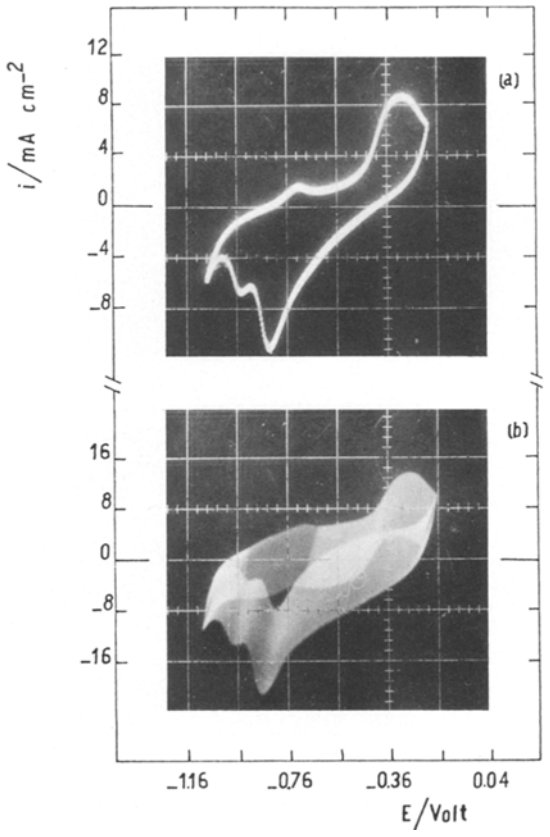

Fig. 6. RTPS and TMTPS *E–I* displays recorded in Fe/0.1 N KOH. (a) $v = 0.2\,V\,s^{-1}$; (b) $v_b = 0.2\,V\,s^{-1}$, $v_m = 20\,V\,s^{-1}$, $\Delta E_m = 0.06\,V$.

ΔE_m and a large v_m/v_b ratio (Fig. 6b) presents only a relaxation effect due to the diffusion contribution in the electrical double layer. On increasing ΔE_m and decreasing the v_m/v_b ratio (Fig. 7) two cathodic current contributions are noticed during the positive-going potential scan together with a hardly distinguishable anodic hump just in the potential range preceding peak I. Likewise, the negative-going potential scan exhibits at least three conjugated redox couples in the $-0.5\,V$ to $-1.15\,V$ range. At potentials within the potential range of current peak II the electrochemical reaction behaves as a completely irreversible process.

Comparative runs made with 0.1 N KOH solution in the presence and in the absence of supporting electrolyte reveal a change in the relative contribution of the various conjugated redox systems in the overall TMTPS contour.

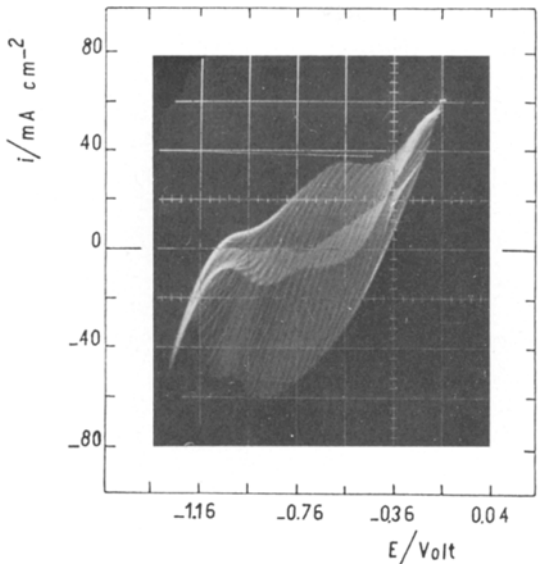

Fig. 7. E–I profile run with TMTPS in 0.1 N KOH. v_b = 2 V s^{-1}, v_m = 20 V s^{-1}, ΔE_m = 0.2 V.

Thus, in the presence of the supporting electrolyte, both the peak I to peak II and the peak V″ to peak IV height ratios are increased. The E–I profiles obtained with TMTPS when $E_{s,a}$ is gradually increased (Fig. 8a) show the genesis of the cathodic current peaks along the positive-going potential excursion. A faster response of the electrochemical system is observed when the $E_{s,a}$–$E_{s,c}$ potential range is confined to that of current peaks IIa and IIc. Then, both anodic and cathodic current contributions are larger than those recorded within wider $E_{s,a}$–$E_{s,c}$ potential ranges and the fine structure of the current peaks is hardly distinguishable.

Under comparable TMTPS, the E–I contours obtained in the presence of 0.6 N K_2SO_4 show fine structure and the corresponding conjugated electrochemical reactions appear more clearly defined than those recorded in the absence of the supporting electrolyte. The presence of the latter reflects clearly on the influence of ΔE_m, at constant v_b and v_m, to decrease the diffuse double-layer relaxation effect (Figs. 8b and c) and, correspondingly, to achieve a clearer definition of the different Faradaic contributions along the potential scans.

The RTPS E–I profile run under comparable potential perturbation conditions with the

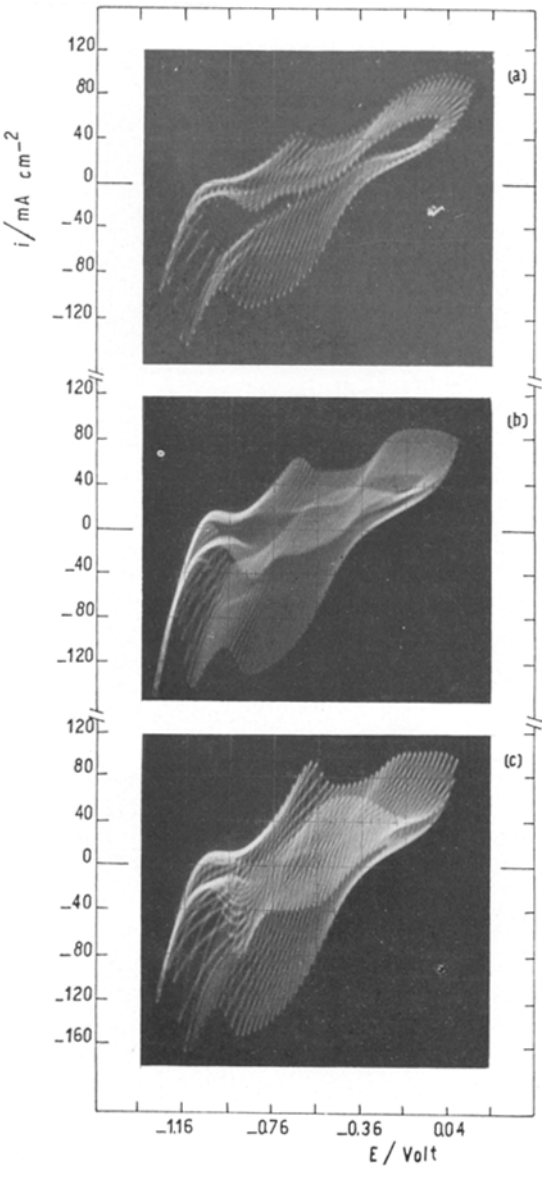

Fig. 8. Influence of v_m and ΔE_m on the E–I profiles run with TMTPS in 0.1 N KOH + 0.6 N K_2SO_4 at v_b = 2 V s^{-1}. (a) v_m = 25 V s^{-1}, ΔE_m = 0.23 V; (b) v_m = 50 V s^{-1}, ΔE_m = 0.23 V; (c) v_m = 50 V s^{-1}, ΔE_m = 0.36 V.

Fe/0.01 N KOH + 0.66 N K_2SO_4 interface is qualitatively similar to those recorded at higher KOH concentrations (Fig. 9). The same number of current peaks and humps are observed, but their potentials are shifted about 0.120 V towards the positive potential side when compared to the E–I display run with the 1 N KOH solution. Similar

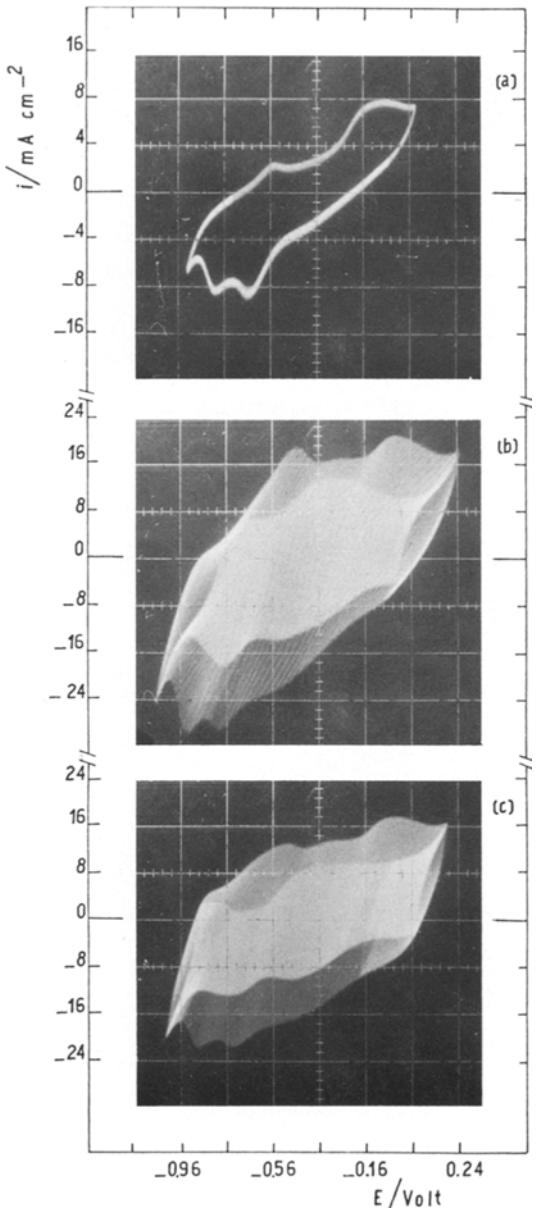

Fig. 9. Comparison between RTPS and TMTPS voltammograms in 0.01 N KOH + 0.66 N K_2SO_4. (a) $v = 0.2\,V\,s^{-1}$; (b) $v_b = 0.2\,V\,s^{-1}$, $v_m = 20\,V\,s^{-1}$, $\Delta E_m = 0.3\,V$; (c) $v_b = 0.2\,V\,s^{-1}$, $v_m = 50\,V\,s^{-1}$, $\Delta E_m = 0.15\,V$.

conclusions are derived from the corresponding TMTPS *E–I* displays.

4. Discussion

Potentiodynamic runs made with the Fe/alkaline solution interfaces in the potential range between the hydrogen and oxygen evolution reactions reveal a multiplicity of current peaks, both anodic and cathodic, associated with the participation of Fe(0), Fe(II) and Fe(III) species in different electrochemical reactions [1, 2, 4, 5, 8–12, 18, 21, 27]. The corresponding *E–I* profile depends upon the composition of the electrolyte [16, 28, 29], the alkali concentration [11, 30, 21], the temperature [2, 10, 21, 32] and the impurity characteristics of the metal. Thus the presence of Li^+ hinders the formation of the passivating species and decreases the hydrogen evolution overvoltage [33]. Comparable effects result when the electrolyte is saturated with either $Ca(OH)_2$, $Ba(OH)_2$ or $Mg(OH)_2$ [29] and when impurities such as Mg, V and Ti are present in the iron [34]. The composition and structure of the passivating film, as well as the formation of soluble Fe(II) and Fe(III) species, also depend upon the electrolyte concentration and temperature [3, 5, 18, 27, 35–38]. On the other hand, the results obtained with either potentiostatic or galvanostatic perturbation techniques, as well as low potential sweep rates, usually involve a relatively large charge so that the response of the system is to a great extent associated with the growth of the passivating layer [10–12, 15, 20, 35]. Therefore, the mechanistic conclusions from the previous studies, although consistent with the present experiments, are difficult to generalize because the response of the electrochemical process depends upon the time scale of the electrical perturbation function.

The conventional RTPS *E–I* displays run between $E_{s,c} = -1.2\,V$ and $E_{s,a} = -0.2\,V$, at $0.2\,V\,s^{-1}$, exhibit three anodic current peaks (I, II and III), a small anodic shoulder (III′) and two cathodic current peaks (IV and V) and a shoulder (IV′). In earlier studies the new phase formation under RTPS perturbation conditions was related to the presence of different oxohydroxo-containing iron species under nonequilibrium conditions. The correlation of the different current peaks with possible conjugated redox processes was made on the basis of the thermodynamic properties of the different reactants and products which are identified through the use of optical techniques [3, 14, 16]. However, this interpretation is ambiguous particularly when it is applied to the initial stages of the film growing process.

Within the potential range where the anodic

current peaks I and II are recorded, the main processes are associated with the formation of Fe(I) intermediate species and Fe(II) species. The corresponding processes can be discussed in more detail through the analysis of the TMTPS contours (Fig. 2b). The *E–I* profile extending from −1.0 V up to −0.9 V involves relatively symmetric anodic and cathodic current contributions, which produce a hardly distinguishable anodic hump at the negative potential side of current peak I and a broad cathodic current peak defined at −0.9 V. The latter, as observed in the positive-going potential TMTPS contour, is closely located in the same potential range of the cathodic current peak IV. In this potential range the anodic dissolution of iron in the electrolyte takes place [27].

The initial Fe(II) electroformation in alkaline solutions can be formally described by the mechanism involving consecutive electron transfer and chemical reactions [16, 17]. Therefore, the initiation of the anodic reaction can be formally expressed as

$$Fe + OH^- = Fe(OH^-)_{ad} \quad (1a)$$

$$Fe(OH^-)_{ad} = Fe(OH)_{ad} + e. \quad (1b)$$

Step 1a represents the anion adsorption equilibrium on the metal surface and Step 1b appears as a fast electron-transfer process in the TMTPS contour within the −1.0 V to −0.9 V potential range. Likewise when the potential limit extends to −0.8 V, the anodic current peak I and the cathodic current peak at ~−0.9 V are distinguishable. The corresponding conjugated redox processes can be related to the reaction following step 1, namely

$$Fe(OH)_{ad} = (FeOH)^+ + e. \quad (2)$$

Reaction 2 has been postulated as the rate-determining step in the stationary corrosion of iron in aqueous solutions, either acid, neutral or alkaline [16, 17, 39–41]. The irreversibility of Step 2 explains why, in the positive-going TMTPS contour (−0.7 V to −0.5 V range), the anodic charge is appreciably greater than the corresponding cathodic charge. However, the electrochemical behaviour of iron in the alkaline electrolytes, including the fate of the initial $Fe(OH)_{ad}$ species in the formation of either soluble or insoluble species, is strongly dependent on both the potential and the electrolyte concentration, as can be concluded from the recent electroreflection spectra of iron in the alkaline solution concerning the strong water–metal interaction at the interface [21, 27, 42, 43].

In the TMTPS contours between −0.5 V and −0.4 V, no net cathodic charge is seen, but at potentials hardly more negative than −0.5 V (Figs. 2 and 3) the cathodic envelope of the positive-going potential TMTPS *E–I* display shows a clear hump which should be related to the partial electroreduction of the initial Fe(III) species preceding the appearance of the main anodic current peak at ~−0.2 V. On extending the potential towards values more positive than −0.4 V, a net anodic charge can be distinguished which corresponds to the appearance of the anodic current peak in the RTPS *E–I* display. This current contribution has already been assigned to the irreversible formation of Fe(III) species. The major irreversibility, is however, observed at −0.4 V or thereabouts (Fig. 4). In the −0.3 V to −0.1 V range the electrochemical system exhibits an apparent faster response but it also involves another anodic current hump at ~−0.2 V.

The negative-going potential TMTPS *E–I* display at $1\,V\,s^{-1}$ presents the major irreversibility in the −0.7 V to −0.9 V range, where the cathodic current peak IV is well defined although it is apparently preceded by a small hump at ~−0.75 V (Fig. 6). Finally, at potentials more negative than −0.9 V, the small contribution of an apparently irreversible conjugated redox system can also be distinguished before reaching the H_2 evolution region. The correspondence of the anodic and cathodic currents related to the various conjugated processes is confirmed through the change of the amplitude and the frequency of the modulating signal.

The irreversible characteristic of the electrochemical reaction is also related to the hysteresis loop of the *E–I* display of each modulating cycle. During the positive-going potential *E–I* display, the irreversibility of the reaction increases when the potential extends beyond −0.5 V. Otherwise, during the negative-going potential *E–I* display the greater irreversibility is observed when the potential sweep extends more negative than −1.1 V (Figs. 3 and 8). This suggests that in the potential range of the Fe(II) to Fe(III) electrochemical reactions at least two different processes

can be distinguished. Thus, the *E–I* response during the positive potential scan can be explained through the electro-oxidation of $Fe(OH)_2$ species yielding FeOOH species followed by a chemical reaction which can be formally expressed as:

$$[Fe(OH)_2]_{av} \rightleftharpoons [FeOOH]_u + H^+ + e \quad (3a)$$

$$[Fe(OH)_2]_{av} \rightleftharpoons [FeOOH]_s + H^+ + e \quad (3b)$$

where the properties of the reactant depend on its formation conditions and history. This is denoted by the subscript 'av'. The electro-oxidation yields either the s- (stable) or the u- (unstable) species. The latter transforms spontaneously into the s-species. The different species represented by the chemical formula in brackets should correspond to complex chemical structures such as those found for the $Ni(OH)_2/NiOOH$ redox system. They may involve a different water content in the film and also a change of the crystallographic configuration.

The reactions occurring during the negative-going potential scan can be represented in an analogous way, as follows:

$$H^+ + e + [FeOOH]_{av} \rightleftharpoons [Fe(OH)_2]_u \quad (4a)$$

$$H^+ + e + [FeOOH]_{av} \rightleftharpoons [Fe(OH)_2]_s \quad (4b)$$

where 'av' denotes the average reactivity of the Fe(II) and Fe(III) film-forming species, which depends on the potential perturbation conditions, and u and s denote again the unstable and stable species, respectively. The ratio of the s- to the u-species in each case depends upon the time scale of the perturbation function.

On the other hand, the fine structure of the TMTPS profiles shows the occurrence of relatively more reversible reactions in the potential range of Reactions 3 and 4, which can be probably represented as

$$[Fe(OH)_2]_u = [FeOOH]_u + H^+ + e \quad (5)$$

when the potential moves in the anodic direction; the reverse reaction takes place when the potential is swept towards negative values. Correspondingly, as part of the $[Fe(OH)_2]_u$ transforms into $[Fe(OH)_2]_s$, the electro-reduction of the latter according to

$$[Fe(OH)_2]_s = [FeOOH]_u + H^+ + e \quad (6)$$

becomes feasible. Reaction 6 should be related to the more irreversible profile located at potentials lower than −0.94 V. Consequently, Reactions 1 to 6, including new phase formations and probably phase transitions, account for the large number of conjugated redox systems found in the transient response of the Fe/alkaline solution interfaces.

The conversions of the u-species into the s-species play a definite role in the ageing of the oxygen-containing species produced at the electrochemical interface. Therefore, the overall electrochemical reactions related to the Fe/KOH solution interfaces, in the concentration range between 10^{-2} M to 1 M involves the participation of electrochemical and chemical reactions in a reaction pathway which essentially is similar to that recently proposed to explain the electrochemical behaviour of the Ni/KOH solution interfaces [26, 44–46].

Nevertheless, the present results preclude establishing any correlation between the different species and the structure of those recognized through the application of optical techniques [3, 14, 16, 22, 47]. The ageing processes which are assisted to some extent by the potentiodynamic perturbation, are in part related to the change of the volume ratio in the solid phases involved in the electrochemical conversions. In the literature this effect has been referred to the marked porosity of the Fe electrode, as the volume of the solid phase expands about four times during the conversion of Fe into $Fe(OH)_2$ [48]. But the main ageing effects may be due to a dehydration and simultaneous Fe(II) formation in the hydrated films. The creation of anionic vacancies would increase the overall polarization resistance, as in the case of the electrical conductivity of FeOOH [49]. A mechanism of this type probably applies to the hydrated oxygen-containing films anodically formed on the iron group metals.

Acknowledgements

INIFTA is sponsored by the Consejo Nacional de Investigaciones Científicas y Técnicas, the Universidad Nacional de La Plata and the Comisión de Investigaciones Científicas (Provincia de Buenos Aires). This works was also partially sponsored by the Regional Program for the Scien-

tific and Technological Development of the Organization of the American States and the SENID (Navy Research and Development Service of Argentina).

References

[1] J. Labat, J. C. Jarrousseau and J. F. Laurent, *Proc. 7th Power Sources Symp. Brighton* (1970) p. 283.
[2] D. D. MacDonald and D. Owen, *J. Electrochem. Soc.* **120** (1973) 317.
[3] L. Öjefors, *ibid* **123** (1976) 1691.
[4] R. S. Schrebler Guzmán, J. R. Vilche and A. J. Arvía, *Electrochim. Acta* **24** (1979) 395.
[5] R. D. Armstrong and I. Baurhoo, *J. Electroanal. Chem.* **34** (1972) 41.
[6] C. M. Shepherd and S. Schuldiner, *J. Electrochem. Soc.* **119** (1972) 572.
[7] C. T. Franklin and A. M. Wong, *Denki Kagaku* **38** (1970) 90.
[8] V. N. Flerov and L. I. Pavlova, *Elektrokhim.* **3** (1967) 621.
[9] D. Geana, A. A. El Miligy and W. J. Lorenz, *J. Appl. Electrochem.* 4 (1974) 337.
[10] B. Andersson and L. Öjefors, *J. Electrochem. Soc.* **123** (1976) 824.
[11] D. D. MacDonald and B. Roberts, *Electrochim. Acta* **23** (1978) 781.
[12] D. W. Shoesmith, P. Taylor, M. G. Bailey and B. Ikeda, *ibid* **23** (1978) 903.
[13] A. M. Sukhotin and K. M. Kartashova, *Corrosion Sci.* **5** (1965) 393.
[14] H. G. Silver and E. Lekas, *J. Electrochem. Soc.* **117** (1970) 5.
[15] S. Asakura and K. Nobe, *ibid* **118** (1971) 536.
[16] Y. Geronov, T. Tomov and S. Georgiev, *J. Appl. Electrochem.* **5** (1975) 351.
[17] B. Kabanov, R. Burstein and A. Frumkin, *Disc. Faraday Soc.* **1** (1947) 259.
[18] H. Cnobloch, D. Gröppel, W. Nippe and F. von Sturm, *Chem. Ing. Tech.* **45** (1973) 203.
[19] A. P. P'yankova and Z. A. Iofa, *Elektrokhim.* **10** (1974) 1344.
[20] D. D. MacDonald and B. Roberts, *Electrochim. Acta* **23** (1978) 557.
[21] G. J. Bignold, *Proc. NACE-4, Surrey, UK 1973* (published 1976).
[22] I. Olefjord, *J. Appl. Electrochem.* **5** (1975) 145.
[23] R. S. Schrebler Guzmán, J. R. Vilche and A. J. Arvía, *Electrochim. Acta* submitted for publication.
[24] B. E. Conway, H. Angerstein-Kozlowska, F. C. Ho, J. Klinger, B. MacDougall and S. Gottesfeld, *Faraday Disc. Chem. Soc.* No. 56 (1973). p. 210.
[25] N. R. de Tacconi, J. O. Zerbino and A. J. Arvía, *J. Electroanal. Chem.* **79** (1977) 287.
[26] R. S. Schrebler Guzmán, J. R. Vilche and A. J. Arvía, *J. Appl. Electrochem.* **9** (1979) 321.
[27] R. D. Armstrong and I. Baurhoo, *J. Electroanal. Chem.* **40** (1972) 325.
[28] N. A. Hampson, R. J. Latham, A. Marshall and R. D. Giles, *Electrochim. Acta* **19** (1974) 397.
[29] S. Yu. Volosova, Z. A. Iofa and T. G. Stepina, *Elektrokhim.* **13** (1977) 393.
[30] T. Nota, K. Kudo and N. Sato, *Nippon Kinzoku Gakkaishi* **37** (1973) 1088.
[31] R. B. Diegle and D. A. Vermilyea, *J. Electrochem. Soc.* **122** (1975) 180.
[32] W. M. M. Huybregts, G. Van Osch and A. Snel, in *Proc. 4th Int. Congr. Metal Corrosion, NACE, Houston 1969* (edited by N. E. Hammer) (1972) p. 501.
[33] N. A. Hampson, R. J. Latham, A. N. Oliver, R. D. Giles and P. C. Jones, *J. Appl. Electrochem.* **3** (1973) 61.
[34] T. N. Glazatova, A. M. Novakovskii, G. G. Drachev and N. N. Baikova, *Sb. Khim. Istochnikam. Toka Nauch. Issled Akkumulyater Inst.* **6** (1971) 79.
[35] G. J. Bignold, *Corrosion Sci.* **12** (1972) 145.
[36] F. I. Kukoz and A. A. Emetts, *Tr. Novocherkassk. Politekh. Inst.* **269** (1972) 61.
[37] H. Kubsch, E. Fritzsch and H. A. Schneider, *Neue Hütte* **19** (1974) 303.
[38] A. Howe and K. Gallagher, *J. Chem. Soc. Faraday I* **71** (1975) 22.
[39] J. O'M. Bockris, D. Drazic and A. R. Despic, *Electrochim. Acta* 4 (1961) 325.
[40] E. J. Kelly, *J. Electrochem Soc.* **112** (1965) 124.
[41] W. J. Lorenz and J. R. Vilche, *Corrosion Sci.* **12** (1972) 785.
[42] Ya. M. Kolotyrkin, R. M. Lazorenko-Manevich, L. A. Sokolova and V. G. Plotnikov, *Electrokhim.* **14** (1978) 344.
[43] P. Doig and P. E. J. Flewitt, *Corrosion Sci.* **17** (1977) 369.
[44] R. S. Schrebler Guzmán, J. R. Vilche and A. J. Arvía, *J. Electrochem. Soc.* **125** (1978) 1578.
[45] J. R. Vilche and A. J. Arvía, in 'Passivity of Metals' (edited by R. P. Frankenthal and J. Kruger) The Electrochemical Society, New Jersey (1978) p. 861.
[46] R. S. Schrebler Guzmán, J. R. Vilche and A. J. Arvía, *J. Appl. Electrochem.* **9** (1979) 183.
[47] A. J. Salkind, C. J. Venuto and S. U. Falk, *J. Electrochem. Soc.* **111** (1964) 493.
[48] A. M. Novakovskii, S. A. Grushkina and R. L. Kozlova, *Zh. Prikl. Khim.* **46** (1973) 2183.
[49] K. Kaneko and K. Inouye, *J. Chem. Soc. Faraday I* **72** (1976) 1258.